Atmos. Meas. Tech. Discuss., 6, 4999–5031, 2013
www.atmos-meas-tech-discuss.net/6/4999/2013/
doi:10.5194/amtd-6-4999-2013

Atmospheric Measurement Techniques Discussions

Remote sensing of atmospheric trace gas columns: an efficient approach for regularization and calculation of total column averaging kernels

T. Borsdorff, O. P. Hasekamp, A. Wassmann, and J. Landgraf

SRON – Netherlands Institute for Space Research, Utrecht, the Netherlands

Received: 27 March 2013 – Accepted: 27 May 2013 – Published: 5 June 2013

Correspondence to: T. Borsdorff (t.borsdorff@sron.nl)

Published by Copernicus Publications on behalf of the European Geosciences Union.

Abstract

A concept is proposed to retrieve the vertical column densities of atmospheric trace gases from remote sensing measurements. It combines the numerical simplicity of a least-squares profile scaling retrieval with the numerically robust calculation of the total column averaging kernel using an analytic expression. The approach enables calculation of the total column averaging kernel on arbitrary vertical grids. Formally, the proposed method is equivalent to Tikhonov regularization of the first kind with an infinite regularization strength. Due to its efficiency it is particularly suited for implementation in operational data processing with high demands on processing time. To demonstrate the method, we apply it to CO column retrieval from simulated measurements in the 2.3 µm spectral region and to O_3 column retrieval from the UV, which represents ideal measurements of a series of space-borne spectrometers like SCIAMACHY, TROPOMI, GOME, and GOME-2. For both spectral ranges, we consider clear-sky and cloudy scenes where clouds are modelled as an elevated Lambertian surface. Here, the smoothing error for the clear-sky and cloudy atmosphere is significant and reaches several percent, depending on the reference profile which is used for scaling. This underlines the importance of the column averaging kernel for a proper interpretation of retrieved column densities. Furthermore, we show that the total column smoothing error is affected by a discretization error when total column averaging kernels are not represented on a fine enough vertical grid. For both retrievals this effect becomes negligible by using a vertical grid with 20–40 equally thick layers between 0 and 50 km.

1 Introduction

Measurements of the vertically integrated column density of atmospheric trace gases provide scientifically valuable information. They are primarily obtained by remote sensing techniques from ground and space. Satellite measurements provide global information about the vertically integrated column density of atmospheric trace gases.

AMTD
6, 4999–5031, 2013

In the ultraviolet, radiance measurements of several space borne spectrometers (e.g. Solar backscattered Ultra Violet – SBUV – instrument, Bhartia et al., 2012; the Global Ozone Monitoring Experiment – GOME, Burrows et al., 1999; and SCIAMACHY, Bovensmann et al., 1999) have demonstrated the unique ability to measure the vertical integrated column density of several trace gases (e.g. NO_2, Richter and Burrows, 2002, and O_3, Lerot et al., 2010). In the short-wave infrared, measurements of SCIAMACHY and the Greenhouse Gases Observing Satellite (GOSAT) provide information on the total column of CH_4 and CO_2 (Frankenberg et al., 2006; Butz et al., 2011; Schepers et al., 2012; Frankenberg et al., 2011). In addition, SCIAMACHY measurements around 2.3 µm are used to retrieve the total column densities of CO (Buchwitz and Burrows, 2004; Gloudemans et al., 2008; Frankenberg et al., 2005).

From ground, long-term measurements of vertically integrated column densities of atmospheric trace gases have been performed in the UV, VIS, SWIR and Mid-IR by Dobson and Brewer, DOAS and FTIR spectrometers. The atmospheric abundance of several trace gases are retrieved (e.g. O_3, Schneider et al., 2008; Barret et al., 2002; HNO_3, Vigouroux et al., 2007; Griesfeller et al., 2005; CO, Yurganov et al., 2005, 2004; Borsdorff and Sussmann, 2009; Rinsland et al., 2002; Pougatchev and Rinsland, 1995; CO_2, Yang et al., 2002; CH_4, Angelbratt et al., 2011; Washenfelder et al., 2003). For SWIR and Mid-IR range this measurements are provided by the IRWG and TCCON network.

A trace gas column retrieval represents a typical inversion problem of atmospheric remote sensing which is usually limited in its vertical sensitivity. This means an unregularized profile retrieval based on a standard least-squares fit yields a trace gas profile which is dominated by the contribution of measurement noise. Thus, the retrieval of such a profile is ill-posed and requires regularization to obtain a stable solution. In practice there are two common ways to regularize the least-squares solution. First, a vertical trace gas profile is retrieved using a Tikhonov regularization approach or optimal estimation to stabilize the inversion. Subsequently, the retrieved profile and the profile averaging kernel are vertically integrated. So, an analytical expression is given

AMTD
6, 4999–5031, 2013

for the column averaging kernel which describes the sensitivity of the retrieved column with respect to changes of the true vertical trace gas distribution as function of altitude. In an ideal case, the column averaging kernel is constant with altitude, representing a retrieval product which corresponds to the geometrical integration of the true trace gas profile. In practice, the column averaging kernel shows an altitude dependence. Mainly due to atmospheric scattering and the temperature dependence of atmospheric absorption, the retrieved column can be described by an altitude integration of the true profile weighted with the column averaging kernel. Despite its theoretical advantages, only a few retrieval algorithms use this approach, notably RemoteC (Butz et al., 2010) and ACOS (O'Dell et al., 2012). The reason for this could be the numerical complexity of the approach and its dependence on the particular regularization of the cost function.

More frequently used is a regularization approach which selects ad hoc the most representative vertical profile which is normalized to its vertical column amount. Subsequently a scaling factor of this profile is determined by a standard least-squares fit. For the interpretation of satellite observations, this technique is employed e.g. by Gloudemans et al. (2008) for CO column retrieval from SCIAMACHY measurements in the shortwave infrared at around 2.3 µm and by Lerot et al. (2010) for ozone column retrieval from GOME-2 measurements. Furthermore, this method is the official retrieval approach for the considered species of the TCCON network. Hence, this retrieval approach is capable to produce column measurements of trace gases with high precision which even fulfill the strong requirements of the TCCON network (Wunch et al., 2010). The implementation of this approach is straightforward and its numerical performance is beneficial with respect to computation time. But its main drawback is the lack of the corresponding column averaging kernel.

Eskes and Boersma (2003) have derived a method to determine column averaging kernels for the Differential Optical Absorption Spectroscopy (DOAS) method, which is applicable for optically thin absorbers. A corresponding method for a column retrieval using profile scaling is no yet reported. Buchwitz and Burrows (2004) have estimated the column averaging kernel by a numerical perturbation of a least-squares

AMTD
6, 4999–5031, 2013

fitting approach. Although valid in general, such an approach can only be applied to a few cases which are assumed to be representative for the overall retrieval product. Furthermore, the accuracy of the numerical perturbation requires a careful tuning of the perturbation strength and may result in numerical instability. Thus, for operational data processing this approach cannot be applied.

In this study, we present a concept for the retrieval of vertically-integrated column densities of atmospheric trace gases from remote sensing measurements which is based on the least-squares scaling of an reference profile but provides, in addition, an analytical expression for the column averaging kernel. We will show that the proposed approach is equivalent to a profile retrieval approach using Tikhonov regularization of first order for an infinite regularization strength with all advantages of a robust numerical implementation of the least-squares scaling approach. Thus the proposed approach combines the advantages of both regularization strategies, providing an analytical expression for the column averaging kernel with a straightforward numerical implementation. Due to that the approach is suited in particular for operational data processing. The paper is structured as followed: in Sect. 2.1 we summarize Tikhonov regularization of first order and Sect. 2.2 discusses the generalized singular value decomposition for the clear representation of the regularized solution. This allows us to discuss the profile scaling approach in the context of Tikhonov regularization in Sect. 2.3, which leads us to the aspired formulation of the column averaging kernel. The application to CO and O_3 column retrieval is discussed in Sect. 3 which provide further insides in the interpretation of the profile scaling approach. The same section addresses the representation error of the column averaging kernel. Finally, Sect. 4 summarizes the paper and states its conclusions.

AMTD
6, 4999–5031, 2013

2 Inversion problem solved by regularization

2.1 Tikhonov regularization

To retrieve information about the abundance of an atmospheric trace gas from a measurement $\boldsymbol{y}_{\text{meas}}$ of spectral dimension m, we employ a forward model $\boldsymbol{F}$ which describes the measurement within the bounds of a spectral error $\boldsymbol{e}_y$, namely

$$\boldsymbol{y}_{\text{meas}} = \boldsymbol{F}(\boldsymbol{x}) + \boldsymbol{e}_y. \quad (1)$$

Here, the n imensional state vector $\boldsymbol{x}$ represents the vertical distribution of a trace gas. After a Taylor expansion of $\boldsymbol{F}$ around a first guess profile $\boldsymbol{x}_0$, Eq. (1) can be written as:

$$\boldsymbol{y} = \mathbf{K}\boldsymbol{x} + \boldsymbol{e}_y \quad (2)$$

with $\boldsymbol{y} = \boldsymbol{y}_{\text{meas}} - \boldsymbol{F}(\boldsymbol{x}_0) + \mathbf{K}\boldsymbol{x}_0$ and the Jacobian or kernel matrix $\mathbf{K} = \partial \boldsymbol{F}/\partial \boldsymbol{x}(\boldsymbol{x}_0)$. Furthermore, we assume that the measurement noise is described by a nonsingular measurement error covariance matrix $\mathbf{S}_{\text{e}} \in \mathbb{R}^{m\times m}$. The retrieval of a trace gas abundance involves finding a state vector $\widehat{\boldsymbol{x}}$ which reproduces the measurement $\boldsymbol{y}$ within its error bounds via the forward model $\boldsymbol{F}$. This inversion of Eq. (2) represents an ill-posed problem and so no unique solution exists. In other words, a standard least-squares fit of the forward model to the measurement would yield a profile which is dominated by noise contributions. Thus, to reduce the noise propagation on the solution the least-squares solution has to be regularized. For this purpose, we employ the Tikhonov regularization technique (Phillips, 1962; Tikhonov, 1963; Twomey, 1963). The inverse problem can than be formulated as a minimisation problem of the following cost function:

$$\widehat{\boldsymbol{x}}_{\text{reg}} = \min_{x} \{ \| \mathbf{S}_{\text{e}}^{-1}(\mathbf{K}\boldsymbol{x} - \boldsymbol{y}) \|^2 + \lambda^2 \| \mathbf{L}_{n-p}(\boldsymbol{x} - \boldsymbol{x}_{\text{a}}) \|^2 \} \quad (3)$$

where $\| \cdot \|$ represents the L_2 norm. The rationale for the side constraint in Eq. (3) is to reduce the noise propagation on the solution and at the same time to extract as

AMTD
6, 4999–5031, 2013

much information as possible from the measurement. Here, the difference between the state vector $\boldsymbol{x}$ and an a priori state vector $\boldsymbol{x}_a$ is weighted by a smoothing operator $\mathbf{L}_{n-p} \in \mathbb{R}^{p \times n}$, the so-called regularization matrix (Rodgers, 2000). Generally $\boldsymbol{x}_a$ differs from the linearisation point $\boldsymbol{x}_0$ of the forward model. Alternatively, one may choose the side constraint $\lambda^2 \| \mathbf{L}_{n-p} \boldsymbol{x} \|^2$. Common regularization matrices are the unity matrix $\mathbf{L}_0 = \mathbf{I}$ or a discrete version of the first derivative:

$$\mathbf{L}_1(i,j) = \begin{cases} 1, & \text{if } i = j \\ -1, & \text{if } i = j - 1 \\ 0, & \text{else} \end{cases}. \tag{4}$$

The regularization parameter λ balances the two contributions of the cost function shown in Eq. (3) and thus its value is of crucial importance for the inversion. If λ is chosen too large, the noise contribution to the solution of the measurement is low, but the least-squares residual norm deviates significantly from its minimum. On the other hand, if λ is chosen too small, the measurement is fitted well but the solution norm is high, and so, the solution is overwhelmed by noise. Thus, λ should be chosen such that the two contributions of the cost function are well balanced. Such an appropriate value for λ can be found using the L-curve method (Hansen, 1992, 1993).

Formally, the solution of Eq. (3) can be expressed by the gain matrix $\mathbf{G}_{\text{reg}}$,

$$\hat{\boldsymbol{x}}_{\text{reg}} = \mathbf{G}_{\text{reg}} \boldsymbol{y} \tag{5}$$

with

$$\mathbf{G}_{\text{reg}} = \left(\mathbf{K}^T \mathbf{S}_e^{-1} \mathbf{K} + \lambda^2 \cdot \mathbf{L}_{n-p}^T \mathbf{L}_{n-p} \right)^{-1} \mathbf{K}^T \mathbf{S}_e^{-1}. \tag{6}$$

Due to the regularization, the retrieved profile $\hat{\boldsymbol{x}}$ is a smoothed version of the true profile $\boldsymbol{x}_{\text{true}}$. The smoothing can be characterised by the averaging kernel,

$$\mathbf{A} = \frac{\partial \hat{\boldsymbol{x}}}{\partial \boldsymbol{x}_{\text{true}}} = \mathbf{G}_{\text{reg}} \mathbf{K}, \tag{7}$$

AMTD
6, 4999–5031, 2013

and so, the retrieved state vector $\widehat{\boldsymbol{x}}_{\text{reg}}$ in Eq. (5) can be written as:

$$\widehat{\boldsymbol{x}}_{\text{reg}} = \mathbf{A}\,\boldsymbol{x}_{\text{true}} + (\mathbf{I} - \mathbf{A})\,\boldsymbol{x}_{\text{a}} + \boldsymbol{e}_x, \tag{8}$$

where $\boldsymbol{e}_x = \mathbf{G}_{\text{reg}}\,\boldsymbol{e}_y$ represents the error on the retrieved trace gas profile caused by the error $\boldsymbol{e}_y$ on the measurement. The contribution $\mathbf{A}\,\boldsymbol{x}_{\text{true}}$ is the part of the solution which can be determined from the measurement sensitivity, whereas $(\mathbf{I} - \mathbf{A})\,\boldsymbol{x}_{\text{a}}$ is the null space contribution of the solution using a priori knowledge about the atmospheric state. In other words, the measurement is effectively not sensitive to contributions of the null space.

In the following, we use the side constraint $\lambda^2 \,\|\,\mathbf{L}_{n-p}\,\boldsymbol{x}\|^2$ and so Eq. (8) reduces to

$$\widehat{\boldsymbol{x}}_{\text{reg}} = \mathbf{A}\,\boldsymbol{x}_{\text{true}} + \boldsymbol{e}_x. \tag{9}$$

This means that the solution does not include the null space contribution. This representation of the data product is beneficial for its use in data assimilation schemes where one aims to assimilate observations with minimal influence of prior information on the trace gas. When an estimate of the null space contribution is needed, it can be added always to the retrieved state vector after the inversion (Rodgers, 2000). For this reason, we ignore this contribution in the following.

For a proper error characterization of the inversion, the retrieval error covariance matrix $\mathbf{S}_x$ is needed. This can be calculated from the measurement covariance matrix $\mathbf{S}_y$ by

$$\mathbf{S}_x = \mathbf{G}_{\text{reg}}\,\mathbf{S}_y\,\mathbf{G}_{\text{reg}}^T. \tag{10}$$

The column density $\widehat{c}$ of a trace gas is defined by vertical profile integration, namely

$$\widehat{c} = \mathbf{C}^T\,\widehat{\boldsymbol{x}}_{\text{reg}}, \tag{11}$$

where $\mathbf{C} = (f_1, \ldots, f_n)$ represents the corresponding integration. Here, f_k converts the element x_k of the retrieved state vector to the partial column amount of the trace gas

AMTD
6, 4999–5031, 2013

in model layer k. The particular form of f_k depends on the units of state vector $\boldsymbol{x}$ and on the chosen vertical grid. Using this formulation, we can characterize the effect of regularization on the column $\widehat{c}$ by:

$$\widehat{c} = \mathbf{A}_c \boldsymbol{x}_{\text{true}} + e_c, \tag{12}$$

where $\mathbf{A}_c = \mathbf{C}^T \mathbf{A}$ is the column averaging kernel and e_c is the error on the retrieved column. The corresponding null space contribution of an a priori profile $\boldsymbol{x}_a$ is $(\mathbf{C} - \mathbf{A}_c)\boldsymbol{x}_a$. The retrieval noise on the retrieved column is given by the standard deviation

$$\sigma_c = \sqrt{\mathbf{C}^T \mathbf{S}_x \mathbf{C}}. \tag{13}$$

In this manner, all diagnostic tools suited for the retrieval of the state vector $\widehat{\boldsymbol{x}}$ can be transformed to the corresponding diagnostics for the retrieved column $\widehat{c}$.

2.2 A general analytic form for the solution

To study the analytic solution $\widehat{\boldsymbol{x}}$ in Eq. (5), we first transform the cost function (Eq. 3) into an uniform noise representation by substituting $\widetilde{\mathbf{K}} = \mathbf{S}_e^{-1/2}\mathbf{K}$ and $\widetilde{\mathbf{S}}_e = \mathbf{S}_e^{-1/2}\boldsymbol{y}$, which yields

$$\widehat{\boldsymbol{x}} = \min_x \{ \| \widetilde{\mathbf{K}}\boldsymbol{x} - \widetilde{\mathbf{y}} \|_2^2 + \lambda^2 \| \mathbf{L}_{n-p}(\boldsymbol{x}) \|_2^2 \} \tag{14}$$

or

$$\widehat{\boldsymbol{x}} = \widetilde{\mathbf{G}}_{\text{reg}} \widetilde{\mathbf{y}} \tag{15}$$

with

$$\widetilde{\mathbf{G}}_{\text{reg}} = \left(\widetilde{\mathbf{K}}^T \widetilde{\mathbf{K}} + \lambda \mathbf{L}_{n-p}^T \mathbf{L}_{n-p} \right)^{-1} \widetilde{\mathbf{K}}^T. \tag{16}$$

AMTD
6, 4999–5031, 2013

This equation can be simplified using the general single value decomposition (GSVD) of the matrix pair $(\widetilde{\mathbf{K}}, \mathbf{L}_{n-p})$ (Hansen, 1992). For $m \geq n \geq p$, the GSVD of the matrix pair $(\widetilde{\mathbf{K}}, \mathbf{L}_{n-p})$ is

$$\begin{aligned} \widetilde{\mathbf{K}} &= \mathbf{U}\mathbf{D}_K\mathbf{W}^{-1} \\ \mathbf{L}_{n-p} &= \mathbf{V}\mathbf{D}_L\mathbf{W}^{-1} \end{aligned} \tag{17}$$

where the nonsingular matrix $\mathbf{W}^{-1} \in \mathbb{R}^{n\times n}$ represents a new basis of the state space in which both matrices $\widetilde{\mathbf{K}}$, $\mathbf{L}_{n-p}$ can be represented as the diagonal matrices $\mathbf{D}_K \in \mathbb{R}^{n\times n}$, $\mathbf{D}_L \in \mathbb{R}^{p\times n}$. $\mathbf{U} \in \mathbb{R}^{m\times n}$ and $\mathbf{V} \in \mathbb{R}^{p\times p}$ are the corresponding back projections with orthonormal columns $\boldsymbol{u}_i$ and $\boldsymbol{v}_i$, respectively. Therefore, the equations $\mathbf{U}^T\mathbf{U} = \mathbf{I}$, $\mathbf{V}^T\mathbf{V} = \mathbf{I}$, $\widetilde{\mathbf{K}}^T\widetilde{\mathbf{K}} = \mathbf{W}^{-T}\mathbf{D}_K^2\mathbf{W}^{-1}$, and $\mathbf{L}_{n-p}^T\mathbf{L}_{n-p} = \mathbf{W}^{-T}\mathbf{D}_L^T\mathbf{D}_L\mathbf{W}^{-1}$ are valid. The matrices $\mathbf{D}_K$, $\mathbf{D}_L$ are both diagonal matrices of the form

$$\mathbf{D}_K = \begin{pmatrix} \boldsymbol{\Sigma} & 0 \\ 0 & \mathbf{I}_{n-p} \end{pmatrix}, \quad \mathbf{D}_L = (\mathbf{M}, 0) \tag{18}$$

where $\boldsymbol{\Sigma} =$,diag$(\sigma_1, \ldots \sigma_p)$, $\mathbf{M} \in \mathbb{R}^{p\times p}$ hold the corresponding singular values of $(\widetilde{\mathbf{K}}, \mathbf{L}_{n-p})$ and $\mathbf{I}_{n-p} \in \mathbb{R}^{(n-p)\times(n-p)}$ is the unity matrix. As a result, the column vectors $\boldsymbol{w}_i$ of $\mathbf{W}$ for $i = p+1, \cdots n$ span the null space of the regularization matrix $\mathbf{L}_{n-p}$,

$$N\left(\mathbf{L}_{n-p}\right) = \text{span}\left\{\boldsymbol{w}_i, \quad \text{with} \quad i = p+1, \cdots n\right\}. \tag{19}$$

With this decomposition, we can rewrite the gain matrix in Eq. (16) as

$$\widetilde{\mathbf{G}}_{\text{reg}} = \mathbf{W}\left(\boldsymbol{\Phi}\mathbf{D}_K^{-1}\mathbf{U}^T\right) \tag{20}$$

with the diagonal matrix $\boldsymbol{\Phi} = (\mathbf{D}_K^2 + \lambda\mathbf{D}_L^T\mathbf{D}_L)^{-1}\mathbf{D}_K^2$. Equation (16) can also be represented as a linear combination of the column vector $\boldsymbol{w}_j$ of $\mathbf{W}$ since $\boldsymbol{\Phi}_{j,j} = 1$ if $j > p$, namely

AMTD
6, 4999–5031, 2013

$$\widetilde{\mathbf{G}}_{\text{reg}} = \sum_{j=1}^{p} \mathbf{\Phi}_{j,j} \cdot \frac{\boldsymbol{w}_j \boldsymbol{u}_j^T}{\sigma_j} + \sum_{j=p+1}^{n} \boldsymbol{w}_j \boldsymbol{u}_j^T. \tag{21}$$

The filter factor matrix $\mathbf{\Phi}$ reveals how the retrieval result is affected by the regularization strength parameter λ. By choosing $\lambda = 0$, the filter factor matrix becomes $\mathbf{\Phi} = \mathbf{I}$ and therefore

$$\widetilde{\mathbf{G}}_{\text{reg}} = \sum_{j=1}^{p} \frac{\boldsymbol{w}_j \boldsymbol{u}_j^T}{\sigma_j} + \sum_{j=p+1}^{n} \boldsymbol{w}_j \boldsymbol{u}_j^T. \tag{22}$$

This is the gain matrix of the unregularized least-squares fit. By choosing $\lambda \to \infty$, the matrix $\mathbf{\Phi}_{j,j} = 0$ if $j \leq p$ and $\mathbf{\Phi}_{j,j} =$ if $j > p$. Therefore, the gain matrix becomes

$$\widetilde{\mathbf{G}}_{\text{reg}} = \sum_{j=p+1}^{n} \boldsymbol{w}_j \boldsymbol{u}_j^T. \tag{23}$$

That means that the solution space of the minimization problem is equal to the null space $N(\mathbf{L}_{n-p})$ of the regularization matrix. In other words, any state vector of the null space $N(\mathbf{L}_{n-p})$ is not affected by the smoothing of the averaging kernel, i.e.

$$\boldsymbol{x} = \mathbf{A}\boldsymbol{x} \quad \text{for} \quad \boldsymbol{x} \in N\left(\mathbf{L}_{n-p}\right) \quad \text{and for} \quad \lambda \to \infty \tag{24}$$

and so

$$\text{trace}\, \mathbf{A} = n - p \quad \text{for} \quad \lambda \to \infty, \tag{25}$$

which is commonly known as the degrees of freedom for signal of the inversion (dofs).

AMTD
6, 4999–5031, 2013

An important extension to the presented methodology is to use a linear combination of Tikhonov matrices from different order for regularization

$$\mathbf{L} = \sum_{i=1}^{n} \lambda_i \mathbf{L}_{n-i}. \tag{26}$$

For example, by choosing

$$\mathbf{L} = \lambda_1 \mathbf{L}_1 + \lambda_0 \mathbf{L}_0, \quad \text{with} \quad \lambda_1 \to \infty, \quad \lambda_0 \in \mathbb{R} \tag{27}$$

it is possible to force any solution of the inversion to the null space $N(\mathbf{L}_1)$ and additionally constrain the solutions with the lower order Tikhonov matrix $\mathbf{L}_0$. However, in this case the solution space of the minimization problem is not equal to the null space of the regularization matrix $N(\mathbf{L})$. The presented formalism can be straightforwardly generalized to obtain a similar analytical from of the solution for this case.

2.3 Profile scaling retrieval and the total column averaging kernel

Profile scaling retrievals are widely used as described in Sect. 1. Here, a scaling factor of a reference profile is inferred from a measurement via an unregularized least-squares fit. Thus, the inversion relies on an one-parameter least-squares fit of the scaling factor x_{lsq} with the gain matrix

$$\boldsymbol{g}_{\mathrm{lsq}} = \left(\mathbf{K}_{\mathrm{lsq}}^T \mathbf{S}_{\mathrm{e}}^{-1} \mathbf{K}_{\mathrm{lsq}}\right)^{-1} \mathbf{K}_{\mathrm{lsq}}^T \mathbf{S}_{\mathrm{e}}^{-1} \tag{28}$$

and the Jacobian $\mathbf{K}_{\mathrm{lsq}}^T \in \mathbb{R}^m$. This inversion does not provide an analytical approach to calculate the total column averaging kernel. It can be calculated by considering the profile scaling approach as a particular case of Tikhonov regularization of first order for $\lambda \to \infty$ with the gain matrix

$$\widetilde{\mathbf{G}}_{\mathrm{reg}} = \boldsymbol{w}_j \boldsymbol{u}_j^T \tag{29}$$

AMTD
6, 4999–5031, 2013

for $p = n - 1$ in Eq. (23). Here, state vector $\boldsymbol{x}$ is defined as the ratio of the trace gas profile $\boldsymbol{\rho}$ with respect to a reference profile $\boldsymbol{\rho}_{\text{ref}}$, thus

$$\boldsymbol{x} = \boldsymbol{\rho}/\boldsymbol{\rho}_{\text{ref}}. \tag{30}$$

In the following, we show that, although different in dimension, both gain matrices $\boldsymbol{g}_{\text{lsq}}$ and $\widetilde{\mathbf{G}}_{\text{reg}}$ represent the same solution of the inverse problem. The solution, given by the gain matrix $\widetilde{\mathbf{G}}_{\text{reg}}$ in Eq. (29), lies in the null space of the regularization matrix $\mathbf{L}_1$, which is given by $N(\mathbf{L}_1) = \text{span}(\{[1\,1\,1\,\ldots\,1]^T\})$. Thus, the null space of $\mathbf{L}_1$ consists of all state vectors which are constant in altitude and so the gain matrix $\widetilde{\mathbf{G}}_{\text{reg}}$ maps a measurement $\boldsymbol{y}$ to identical element of the state vector. In our case, this is the scaling parameter of the reference profile $\boldsymbol{\rho}_{\text{ref}}$. Consequently, the rows $\boldsymbol{g}_1, \ldots, \boldsymbol{g}_n$ of $\widetilde{\mathbf{G}}_{\text{reg}}$ are identical, $\boldsymbol{g}_1 = \boldsymbol{g}_2 = \cdots = \boldsymbol{g}_n$. Furthermore, because the scaling parameter of the regularization scheme is also retrieved by the one-parameter least-squares fit, we obtain

$$\boldsymbol{g}_i = \boldsymbol{g}_{\text{lsq}} \quad \text{for} \quad i = 1, \cdots, N. \tag{31}$$

Herewith, we can define an analytic method to calculate the total column averaging kernel of a profile scaling retrieval in an efficient and numerically stable way. Furthermore, this method is also valid for constrained profile scaling retrievals since those also fulfill the requirement that any state vector must be part of $N(\mathbf{L}_1)$ and therefore also constant in altitude (see Eq. 27). The recipe can be summarized in three steps:

1. the scaling of a reference profile is retrieved using a standard least-squares fit with associated gain matrix $\boldsymbol{g}_{\text{lsq}}$.

2. on any arbitrary height grid with $n = 1, \cdots, N$ model layers the Tikhonov gain matrix $\widetilde{\mathbf{G}} = (\boldsymbol{g}_1, \boldsymbol{g}_2, \cdots, \boldsymbol{g}_n)^T$ is given by $\boldsymbol{g}_{\text{lsq}}$ with $\boldsymbol{g}_1 = \boldsymbol{g}_2 = \cdots = \boldsymbol{g}_n = \boldsymbol{g}_{\text{lsq}}$.

AMTD
6, 4999–5031, 2013

3. this defines the averaging kernel in Eq. (7) and so the total column averaging kernel in Eq. (12) is given by

$$\mathbf{A}_{\mathrm{col},j} = \boldsymbol{g}_{\mathrm{lsq}}\,\boldsymbol{k}_j \sum_{k=1}^{N} f_k. \tag{32}$$

with the column vector $\boldsymbol{k}_j$ of the Jacobian $\mathbf{K} = (\boldsymbol{k}_1, \cdots, \boldsymbol{k}_N)$ and the conversion factors

$$f_k = \Delta z_k\,\boldsymbol{\rho}_{\mathrm{ref},k}. \tag{33}$$

Here, Δz_k is the geometrical thickness of model layer k and the physical units of the reference profile $\boldsymbol{\rho}_{\mathrm{ref}}$ determines the units of the column density $\widehat{c}$.

To summarize, the presented approach for calculating the total column averaging kernel relies on the numerical implementation of a one-parameter least-squares fit. It is favourable with respect to both numerical implementation and robustness. Furthermore, it provides a straightforward manner to adapt existing algorithms for profile scaling retrieval with minor modifications. The new concept also helps to develop further the results of other studies. For example it eases the calculation of interference errors as presented by Sussmann and Borsdorff (2007) since interference kernels in the profile scaling case can now be calculated directly with an analytical expression without simulating those retrievals first via a Tikhonov regularization (von Clarmann and Grabowski, 2007). This enables the possibility of including such error estimations in the standard output of operational retrieval algorithms.

3 Applications

In this section we apply the proposed method for total column retrieval by profile scaling to two specific satellite remote sensing problems to illustrate the general features of

AMTD
6, 4999–5031, 2013

this kind of retrieval. Moreover, we demonstrate the overall need of the column averaging kernels to interpret correctly the column density retrieved from the measurement. First, we will consider the retrieval of the vertical column density of carbon monoxide (CO) from simulated measurements in the 2.3 µm short wave infrared (SWIR) spectral region. This spectral range is used to determine atmospheric CO abundances from SCIAMACHY SWIR measurements (Gloudemans et al., 2008; Buchwitz and Burrows, 2004, and references therein) and will also be probed by the TROPOMI instrument as payload of the Sentinel 5 Precursor mission (Veefkind et al., 2012), scheduled for launch in 2015. As a second example, we will consider the retrieval of the vertical column density of ozone (O_3) from simulated ultraviolet (UV) measurements as they are done by several space-borne spectrometers, like GOME (Burrows et al., 1999), GOME-2 (Callies et al., 2000), SCIAMACHY (Eskes et al., 2005), OMI (Levelt et al., 2006), and TROPOMI (Veefkind et al., 2012). For this purpose, we assume a nadir viewing geometry of reflected sunlight with a viewing zenith angle of VZA = 0° and a solar zenith angle of SZA = 45°. For SWIR we assume a typical surface albedo of 0.05 and for the UV retrieval a surface albedo of 0.1. The measurements are simulated for clear-sky and cloudy conditions, where clouds are described by an elevated Lambertian surface at 7.5 km altitude with a cloud albedo of 0.5 for SWIR and 0.8 for UV. For partially cloudy scenes the independent pixel approach (e.g. Marshak et al., 1995) is employed with a cloud faction f_{cld}. The model atmosphere is adapted from the US standard atmosphere (NOAA, 1976). Figure 1 shows the simulated measurement under clear-sky conditions for the retrieval windows 2324.5–2338.38 nm for CO and 325.04–334.91 nm for O_3. For the SWIR window, we account for atmospheric absorption by CO, H_2O, HDO, and CH_4. In the UV window, O_3 is considered as the only relevant absorber.

All species in this study are retrieved using the profile scaling approach described in the previous section. CO is retrieved together with the interference species H_2O, HDO, and CH_4 to reduce the interference effect caused by the overlapping absorption lines (Sussmann and Borsdorff, 2007; Borsdorff and Sussmann, 2009; Pougatchev and Rinsland, 1995; Rinsland et al., 2002; Rodgers and Connor, 2003). Ozone is inferred

AMTD
6, 4999–5031, 2013

without accounting for further atmospheric absorbers. For both retrievals, the measurement noise is assumed to be shot noise with a signal to noise ratio of SNR = 100 at the maximum value of the spectrum. Moreover, we also use the profile $\boldsymbol{\rho}_{\text{true}}$ that is used to simulate the measurement spectra as linearisation point for the forward calculation $\boldsymbol{x}_0 = \boldsymbol{\rho}_{\text{true}}$. Thus an iterative inversion approach is not needed to account for the non-linearity of the forward model. Throughout this study, the US standard atmosphere profile will serve as the reference profile $\boldsymbol{\rho}_{\text{ref}}$ in Eq. (30). Hence, the total column averaging kernels of the retrievals are calculated for the true state of the atmosphere $\boldsymbol{\rho}_{\text{true}}$ and are reflective of the vertical sensitivity of a profile scaling retrieval which scales the corresponding US standard profile $\boldsymbol{\rho}_{\text{ref}}$.

The resulting total column averaging kernels for the CO and O_3 retrieval are shown in Fig. 2. Here, we assume that the vertical profile contains partial column densities of the individual layers as its components, which implies that the conversion factor in Eq. (33) is $f_k = 1$. This representation eases the interpretation and it is commonly used in the literature (e.g. Notholt et al., 2000; Borsdorff and Sussmann, 2009; Rodgers and Connor, 2003). The column averaging kernels differ from the ideal case $\widetilde{\mathbf{A}}_c = (1, 1, \cdots, 1)^T$, where $\widetilde{\mathbf{A}}_c \boldsymbol{x}_{\text{true}} = c_{\text{true}}$. For the clear-sky CO retrieval, $\widetilde{\mathbf{A}}_c < 1$ below 5.7 km altitude and $\widetilde{\mathbf{A}}_c > 1$ at higher altitudes. The ozone total column averaging kernel shows a more complex shape with values above and below 1. Only in the range between 21.5 and 29.5 km it is close to its ideal value of unity. For the cloudy case, the retrieved column loses sensitivity to the atmosphere below the cloud but at the same time shows an enhanced retrieval sensitivity above the cloud. This is a typical feature of a profile scaling approach, and it can be explained most easily for the fully clouded scene with cloud faction unity. In this case, the total column is determined by the scaling of the reference profile using only the sensitivity above the cloud and so a change of the trace gas concentration at these altitudes affects the retrieval twice. First, the profile is adapted above the cloud due to the measurement sensitivity and second also below the cloud, although the measurement is not sensitive to this altitude range. This explains the enhanced value of the column averaging kernel above the cloud and also its dependence on cloud height (not

AMTD
6, 4999–5031, 2013

shown). The same rationale is true for the clear-sky and partially cloudy cases, where the altitude ranges of reduced retrieval sensitivity are compensated by enhanced averaging kernel values at other altitudes. It is obvious that only for particular profiles do the differences in the averaging kernel add up such that the retrieved column is equal to the true column. Due to Eq. (24), this is only the case for profiles that can be expressed as a scaling of the reference profile $\boldsymbol{\rho}_{\mathrm{ref}}$, and so the corresponding state vector $\boldsymbol{x}$ is element of the null space $N(\mathbf{L}_1)$. Any other profile has a null space contribution, which means that the retrieved column differs from the true column.

In case that a data product is required that represents an estimate of the true trace gas column, generally one aims to fill up the null space contribution using a proper a priori knowledge of the profile, $(\mathbf{C} - \mathbf{A}_{\mathrm{c}})\,\boldsymbol{x}_{\mathrm{a}}$. One may interpret this term as a correction to the retrieval because the reference profile does not represent the true relative distribution of the trace gas. For example, during the processing of an operational retrieval only a rough estimate of the relative profile is possible. At a later stage due to sophisticated chemical transport modelling the estimate can be improved and so, without reprocessing the measurements, the null space contribution of the model results can be used to correct the retrieval. In this context, it is interesting to note that the reference profile cannot be used for this purpose because of its vanishing contribution to the null space (see Eq. 24).

Thus, the null space or smoothing error $(\mathbf{C} - \mathbf{A}_{\mathrm{c}})\,\boldsymbol{\rho}_{\mathrm{true}}$ of the scaling approach corresponds to the error when the retrieved column is assumed to be an estimate of the true column. To estimate the relevance of the null space contribution, we consider measurement simulations for the set of CO and O_3 profiles shown in Fig. 3. The data set comprises a background and a polluted CO profile, two ozone profiles with low and high stratospheric ozone concentrations and additionally both ozone profiles with an enhanced ozone mixing ratio of 120 ppb for all layers below 2.5 km (not shown), which mimics enhanced ozone concentration in the tropospheric boundary layer. Here, all profiles are scaled to the same vertical column density and as such they differ only in

AMTD
6, 4999–5031, 2013

their relative vertical distribution (not shown in Fig. 3). For the retrieval, the US standard profile is employed as reference profile $\boldsymbol{\rho}_{\text{ref}}$ for scaling.

For the different atmospheric profiles, Tables 1 and 2 summarize the null space error $(\mathbf{C} - \mathbf{A}_c)\,\boldsymbol{\rho}_{\text{true}}$ of the total column for clear-sky atmospheres and the corresponding contribution of particular partial columns. Here, the partial columns are defined over the maximum altitude range such that the averaging kernel is always > 1 or < 1. The vertical domains indicate the ranges where the retrieval either under or overestimates the contribution of the true profile to the true total column. When adding up the partial columns to the total column, errors cancel out to a large extent but overall an error on a percentage level remains for the considered profiles.

The null space error increases significantly when one considers partially cloudy scenes. Figure 4 shows the increase of the total column null space error as a function of the cloud fraction. For a cloud fraction of $f = 0.6$ the additional smoothing error increases to −25 % for the scene of low tropospheric CO concentrations and to −11 % for the polluted scene. For the fully clouded scene the additional error increases to −1 and −14 % respectively. The magnitude of these errors depends on the altitude of the cloud. To demonstrate this, the two cases for CO are recalculated for a cloud placed at 2.5 km and shown in Fig. 4.

Finally, we consider the discretization error of the averaging kernel. Here, the vertical gridding of the averaging kernel is given by the vertical discretization of the Jacobian $\mathbf{K}$ in Eq. (32). As a reference, we use a model atmosphere between 0 and 50 km altitude divided in 512 geometrically equidistant layers. Subsequently, we consider the error in the effective column $\mathbf{A}\,\boldsymbol{x}$ using a vertical grid of N model layers. Figure 5 shows this discretization error as a function of N. Due to the particular form of the column averaging kernel, the discretization error does not always decrease monotonically with increasing number of model layers. However, a representation of the Jacobian on 20–40 layers is sufficient to reduce the discretization error such that it does not represent a significant error source for the different retrievals. Certainly the number of required layers can be further reduced by choosing non-equidistant vertical grids which are particularly

AMTD
6, 4999–5031, 2013

optimized for an specific application, but the general problem of a discretization error cannot be avoided by choosing different grids.

4 Summary and conclusions

In this study, we proposed a concept to retrieve vertical column densities of atmospheric trace gases from remote sensing measurements. The method is based on a least-squares profile scaling approach but it allows one to calculate total column averaging kernels via an analytic expression on arbitrary vertical grids. The approach can be implemented in a straightforward manner, and results in a numerically robust and efficient algorithm. In particular, it is suited for operational data processing with high demands on computation time and also provides a straightforward manner to adapt existing algorithms for profile scaling with minor modifications.

The profile scaling approach represents a particular form of regularization and we showed that for a vertical profile expressed relative to a reference profile, it is equivalent to a Tikhonov regularization of the first kind with an infinite regularization strength. This equivalence allows us to derive an analytical expression for the total column averaging kernel. Moreover, we showed that any unregularized profile scaling retrieval is in general, free from an a priori null space contribution. That is beneficial, in particularly for using the data product in data assimilation schemes where one aims to assimilate observations with a minimal influence of a priori information. As a consequence, the reference profile cannot be used to fill up the null space because by definition it has a vanishing null space contribution.

The proposed regularization scheme is of a general nature and so it can be applied to many retrieval problems using space-borne or ground-based remote sensing measurements. For demonstration, we applied it to the CO column retrievals from simulated spectra in the 2.3 µm region and to O_3 column retrievals in the ultraviolet spectral range. This represents the retrieval concept for a series of space-borne spectrometers like SCIAMACHY, TROPOMI, GOME and GOME-2. For both retrievals, we considered

AMTD
6, 4999–5031, 2013

clear-sky and cloudy scenes where clouds were modelled as an elevated Lambertian surface. We illustrated the dependence of the total column averaging kernel on the cloud coverage of the observed scene. Here, altitudes with a reduced retrieval sensitivity are compensated by enhanced values at other altitudes, which is a typical characteristic of a profile scaling retrieval. So the retrieved column may be interpreted as an estimation of the true vertical column density, even when the measurement is not sensitive for the full altitude range. Consequentially, the smoothing error represents the error due to the fact that the scaled reference profile is not the true profile and so the profile scaling is deficient.

By using the US standard model atmosphere to define the reference profile and by considering both polluted and unpolluted atmospheric abundances and high and low stratospheric ozone for the true profile, we found the smoothing errors for both retrievals in the clear-sky case significant, causing errors of up to −2.83 % of the true vertical column density for CO and 5.37 % for O_3. For cloudy cases with a cloud top at 7.5 km, an additional smoothing error occurs which may reach −30 % for CO and 8 % for O_3, depending on cloud coverage. The particular values of the smoothing error depend on cloud altitude and on the chosen reference profile. In the ideal case, where the relative distributions of the reference and true profiles are equal, the smoothing error will vanish in all cases. However, in practice the use of the total column averaging kernel is essential for the correct interpretation of retrieved data, in particular for cloudy observations. Here it is recommended to represent the column averaging kernel on a vertical grid with 20–40 equally thick layers that extend between 0 and 50 km to avoid significant discretization errors in the estimate of the smoothing error.

The presented algorithm will be used for the operational data processing of CO columns from TROPOMI measurements. Its functionality will be tested on real SCIAMACHY data for the purpose of CO column retrieval and on real GOME-2 data for the purpose of O_3 column estimates in the near future.

AMTD
6, 4999–5031, 2013

Acknowledgements. SCIAMACHY is a joint project of the German Space Agency DLR and the Dutch Space Agency NSO with contribution of the Belgian Space Agency. The work performed is (partly) financed by NSO. The ozonesonde measurements were provided by the World Ozone and Ultraviolet Radiation Data Center (WOUDC). The authors would like to thank Truitt Wiensz for proofreading this work.

References

Angelbratt, J., Mellqvist, J., Blumenstock, T., Borsdorff, T., Brohede, S., Duchatelet, P., Forster, F., Hase, F., Mahieu, E., Murtagh, D., Petersen, A. K., Schneider, M., Sussmann, R., and Urban, J.: A new method to detect long term trends of methane (CH_4) and nitrous oxide (N_2O) total columns measured within the NDACC ground-based high resolution solar FTIR network, Atmos. Chem. Phys., 11, 6167–6183, doi:10.5194/acp-11-6167-2011, 2011. 5001

Barret, B., de Mazière, M., and Demoulin, P.: Retrieval and characterization of ozone profiles from solar infrared spectra at the Jungfraujoch, J. Geophys. Res., 107, 4788, doi:10.1029/2001JD001298, 2002. 5001

Bhartia, P. K., McPeters, R. D., Flynn, L. E., Taylor, S., Kramrova, N. A., Frith, S., Fisher, B., and DeLand, M.: Solar Backscatter UV (SBUV) total ozone and profile algorithm, Atmos. Meas. Tech. Discuss., 5, 5913–5951, doi:10.5194/amtd-5-5913-2012, 2012. 5001

Borsdorff, T. and Sussmann, R.: On seasonality of stratomesospheric CO above midlatitudes: New insight from solar FTIR spectrometry at Zugspitze and Garmisch, Geophys. Res. Lett., 36, L21804, doi:10.1029/2009GL040056, 2009. 5001, 5013, 5014

Bovensmann, H., Burrows, J. P., Buchwitz, M., Frerick, J., Noël, S., Rozanov, V. V., Chance, K. V., and Goedec, A. P. H.: SCIAMACHY: Mission Objectives and Measurement Modes, J. Atmos. Sci., 56, 127–150, 1999. 5001

Brion, J., Chakir, A., Daumont, D., Malicet, J., and Parisse, C.: High-resolution laboratory absorption cross section of O_3, Temperature effect, Chem. Phys. Lett., 213, 610–612, doi:10.1016/0009-2614(93)89169-I, 1993. 5027

Buchwitz, M. and Burrows, J. P.: Retrieval of CH_4, CO and CO_2 total column amounts from SCIAMACHY near-infrared nadir spectra: Retrieval algorithm and first results, Remote Sensing of Clouds and the Atmosphere VIII, Proc. SPIE, 5235, 375–388, 2004. 5001, 5002, 5013

AMTD
6, 4999–5031, 2013

Burrows, J. P., Weber, M., Buchwitz, M., Rozanov, V., Ladstäter-Weißenmayer, A., Richter, A., DeBeek, R., Hoogen, R., Bramstedt, K., Eichmann, K. U., Eisinger, M., and Perner, D.: The global monitoring experiment (GOME): Mission concept and first scientific results, J. Atmos. Sci., 56, 151–175, doi:10.1175/1520-0469(1999)056<0151:TGOMEG>2.0.CO;2, 1999. 5001, 5013

Butz, A., Hasekamp, O. P., Frankenberg, C., Vidot, J., and Aben, I.: CH_4 retrievals from space-based solar backscatter measurements: Performance evaluation against simulated aerosol and cirrus loaded scenes, J. Geophys. Res., 115, D24302, doi:10.1029/2010JD014514, 2010. 5002

Butz, A., Guerlet, S., Hasekamp, O., Schepers, A. G., Aben, I., Frankenberg, C., Hartmann, J. M., Tran, H., Kuze, A., Keppel-Aleks, G. T., Wunch, D., Wennberg, P., Deutscher, N., Griffith, D., Macatangay, R., Messerschmidt, J., Notholt, J., and Warneke, T.: Toward accurate CO_2 and CH_4 observations from GOSAT, Geophys. Res. Lett., 38, L14812, doi:10.1029/2011GL047888, 2011. 5001

Callies, J., Corpaccioli, E., Eisinger, M., Hahne, A., and Lefebvre, A.: GOME-2 – Metop's Second Generation Sensor for Operational Ozone Monitoring, ESA Bulletin, 102, ESTEC, Noordwijk, the Netherlands, 2000. 5013

Eskes, H. J. and Boersma, K. F.: Averaging kernels for DOAS total-column satellite retrievals, Atmos. Chem. Phys., 3, 1285–1291, doi:10.5194/acp-3-1285-2003, 2003. 5002

Eskes, H. J., van der A, R. J., Brinksma, E. J., Veefkind, J. P., de Haan, J. F., and Valks, P. J. M.: Retrieval and validation of ozone columns derived from measurements of SCIAMACHY on Envisat, Atmos. Chem. Phys. Discuss., 5, 4429–4475, doi:10.5194/acpd-5-4429-2005, 2005. 5013

Frankenberg, C., Platt, U., and Wagner, T.: Retrieval of CO from SCIAMACHY onboard ENVISAT: detection of strongly polluted areas and seasonal patterns in global CO abundances, Atmos. Chem. Phys., 5, 1639–1644, doi:10.5194/acp-5-1639-2005, 2005. 5001

Frankenberg, C., Meirink, J. F., Bergamaschi, P., Goede, A. P. H., Heimann, M., Köner, S., Platt, U., Weele, M. V., and Wagner, T.: Satellite chartography of atmospheric methane from SCIAMACHY on board ENVISAT: analysis of the years 2003 and 2004, J. Geophys. Res., 111, D07303, doi:10.1029/2005JD006235, 2006. 5001

Frankenberg, C., Fisher, J. B., Worden, J., Badgley, G., Saatchi, S. S., Lee, J., Toon, G. C., Butz, A., Jung, M., Kuze, A., and Yokota, T.: New global observations of the terrestrial carbon cycle

AMTD
6, 4999–5031, 2013

from GOSAT: Patterns of plant fluorescence with gross primary productivity, J. Geophys. Res., 38, L17706, doi:10.1029/2011GL048738, 2011. 5001

Gloudemans, A. M. S., Schrijver, H., Hasekamp, O. P., and Aben, I.: Error analysis for CO and CH_4 total column retrievals from SCIAMACHY 2.3 μm spectra, Atmos. Chem. Phys., 8, 3999–4017, 2008, http://www.atmos-chem-phys.net/8/3999/2008/. 5001, 5002, 5013

Griesfeller, A., Griesfeller, J., Hase, F., Blumenstock, T., and Nakajima, H.: Comparison of ILAS-II Data With Ground-based FTIR Measurements of O_3, HNO_3, N_2O, and CH_4 Over Kiruna, Sweden, AGU Fall Meeting Abstracts, p. C950, 2005. 5001

Hansen, C.: Analysis of discrete ill-posed problems by means of the L-curve, Soc. Indust. Appl. Math., 34, 561–580, 1992. 5005, 5008

Hansen, C.: The use of the L-curve in the regularization of discrete ill-posed problems, SIAM J. Sci. Comput., 14, 1487–1503, doi:10.1137/0914086, 1993. 5005

Lerot, C., van Roozendael, M., Lambert, J. C., Granville, J., van Gent, J., Loyola, D., and Spurr, R.: The GODFIT algorithm: a direct fitting approach to improve the accuracy of total ozone measurements from GOME, Int. J. Remote Sens., 31, 543–550, doi:10.1080/01431160902893576, 2010. 5001, 5002

Levelt, P. F., van den Oord, G. H. J., Dobber, M. R., Malkki, A., Visser, H., de Vries, J., Stammes, P., Lundell, J. O. V., and Saari, H.: The ozone monitoring instrument, IEEE T. Geosci. Remote, 44, 1093–1101, doi:10.1109/TGRS.2006.872333, 2006. 5013

Levelt, P. F., Veefkind, J. P., Kerridge, B. J., Siddans, R., de Leeuw, G., Remedios, J., and Coheur, P. F.: Observation Techniques and Mission Concepts for Atmospheric Chemistry (CAMELOT), Report 20533/07NL/HE, European Space Agency, Noordwijk, The Netherlands, 2009. 5029

Marshak, A., Davis, A., Wiscombe, W., and Titov, G.: The Verisimilitude of the Independent Pixel Approximation Used in Cloud Remote Sensing, Remote Sens. Environ., 52, 71–78, 1995. 5013

NOAA: U.S. Standard Atmosphere, 1976, Report NOAA-S/T76-1562, National Oceanic and Atmospheric Administration, US Gov. Printing Office, Washington, DC, 1976. 5013, 5029

Notholt, J., Toon, G. C., Rinsland, C. P., Pougatchev, N. S., Jones, N. B., Connor, B. J., Weller, R., Gautrois, M., and Schrems, O.: Latitudinal variations of trace gas concentrations in the free troposphere measured by solar absorption spectroscopy during a ship cruise, J. Geophys. Res., 105, 1337–1350, doi:10.1029/1999JD900940, 2000. 5014

AMTD
6, 4999–5031, 2013

O'Dell, C. W., Connor, B., Bösch, H., O'Brien, D., Frankenberg, C., Castano, R., Christi, M., Eldering, D., Fisher, B., Gunson, M., McDuffie, J., Miller, C. E., Natraj, V., Oyafuso, F., Polonsky, I., Smyth, M., Taylor, T., Toon, G. C., Wennberg, P. O., and Wunch, D.: The ACOS CO_2 retrieval algorithm – Part 1: Description and validation against synthetic observations, Atmos. Meas. Tech., 5, 99–121, doi:10.5194/amt-5-99-2012, 2012. 5002

Phillips, B. C.: A technique for the numerical solution of certain integral equations of the first kind, J. Ass. Comput. Mach., 9, 84–97, doi:10.1145/321105.321114, 1962. 5004

Pougatchev, N. S. and Rinsland, C. P.: Spectroscopic study of the seasonal variation of carbon monoxide vertical distribution above Kitt Peak, J. Geophys. Res., 100, 1409–1416, doi:10.1029/94JD02387, 1995. 5001, 5013

Richter, A. and Burrows, J. P.: Tropospheric NO_2 from GOME measurements, Adv. Space Res., 29, 1673–1683, doi:10.1016/S0273-1177(02)00100-X, 2002. 5001

Rinsland, C. P., Jones, N. B., Connor, B. J., Wood, S. W., Goldman, A., Stephen, T. M., Murcray, F. J., Chiou, L. S., Zander, R., and Mahieu, E.: Multiyear infrared solar spectroscopic measurements of HCN, CO, C_2H_6, and C_2H_2 tropospheric columns above Lauder, New Zealand (45° S latitude), J. Geophys. Res., 107, 4185, doi:10.1029/2001JD001150, 2002. 5001, 5013

Rodgers, C. D.: Inverse Methods for Atmospheres: Theory and Practice, vol. 2, World Scientific, Singapore, New Jersey, London, Hong Kong, 2000. 5005, 5006

Rodgers, C. D. and Connor, B. J.: Intercomparison of remote sounding instruments, J. Geophys. Res., 108, 4116, doi:10.1029/2002JD002299, 2003. 5013, 5014

Rothman, L. S., Barbe, A., Benner, D. C., Brown, L. R., Camy-Peyret, C., Carleer, M. R., Chance, K., Clerbaux, C., Dana, V., Devi, V. M., Fayt, A., Flaud, J.-M., Gamache, R. R., Goldman, A., Jacquemart, D., Jucks, K. W., Lafferty, W. J., Mandin, J.-Y., Massie, S. T., Nemtchinov, V., Newnham, D. A., Perrin, A., Rinsland, C. P., Schroeder, J., Smith, K. M., Smith, M. A. H., Tang, K., Toth, R. A., Vander Auwera, J., Varanasi, P., and Yoshino, K.: The HITRAN molecular spectroscopic database: edition of 2000 including updates through 2001, J. Quant. Spectrosc. Ra., 82, 5–44, doi:10.1016/S0022-4073(03)00146-8, 2003. 5027

Schepers, D., Guerlet, S., Butz, A., Landgraf, J., Frankenberg, C., Hasekamp, O., Blavier, J. F., Deutscher, N. M., Griffith, D. W. T., Hase, F., Kyro, E., Morino, I., Sherlock, V., Sussmann, R., and Aben, I.: Methane retrievals from Greenhouse Gases Observing Satellite (GOSAT) shortwave infrared measurements: Performance comparison of proxy and physics retrieval algorithms, J. Geophys. Res., 117, D10307, doi:10.1029/2012JD017549, 2012. 5001

AMTD
6, 4999–5031, 2013

Schneider, M., Hase, F., Blumenstock, T., Redondas, A., and Cuevas, E.: Quality assessment of O_3 profiles measured by a state-of-the-art ground-based FTIR observing system, Atmos. Chem. Phys., 8, 5579–5588, doi:10.5194/acp-8-5579-2008, 2008. 5001

Sussmann, R. and Borsdorff, T.: Technical Note: Interference errors in infrared remote sounding of the atmosphere, Atmos. Chem. Phys., 7, 3537–3557, doi:10.5194/acp-7-3537-2007, 2007. 5012, 5013

Tikhonov, A.: On the solution of incorrectly stated problems and a method of regularization, Dokl. Acad. Nauk SSSR, 151, 501–504, 1963. 5004

Twomey, S.: On the numerical solution of Fredholm integral equations of the first kind by the inversion of the linear system produced by quadrature, J. Ass. Comput. Mach., 10, 97–101, doi:10.1145/321150.321157, 1963. 5004

Veefkind, J. P., Aben, I., McMullan, K., Forster, H., de Vries, J., Otter, G., Claas, J., Eskes, H. J., de Haan, J. F., Kleipool, Q., van Weele, M., Hasekamp, O., Hoogeveen, R., Landgraf, J., Snel, R., Tol, P., Ingmann, P., Voors, R., Kruizinga, B., Vink, R., Visser, H., and Levelt, P. F.: TROPOMI on the ESA Sentinel-5 Precursor: A GMES mission for global observations of the atmospheric composition for climate, air quality and ozone layer applications, Remote Sens. Environ., 120, 70–83, doi:10.1016/j.rse.2011.09.027, 2012. 5013

Vigouroux, C., De Mazière, M., Errera, Q., Chabrillat, S., Mahieu, E., Duchatelet, P., Wood, S., Smale, D., Mikuteit, S., Blumenstock, T., Hase, F., and Jones, N.: Comparisons between ground-based FTIR and MIPAS N_2O and HNO_3 profiles before and after assimilation in BASCOE, Atmos. Chem. Phys., 7, 377–396, doi:10.5194/acp-7-377-2007, 2007. 5001

von Clarmann, T. and Grabowski, U.: Elimination of hidden a priori information from remotely sensed profile data, Atmos. Chem. Phys., 7, 397–408, doi:10.5194/acp-7-397-2007, 2007. 5012

Washenfelder, R. A., Wennberg, P. O., and Toon, G. C.: Tropospheric methane retrieved from ground based near IR solar absorption spectra, Geophys. Res. Lett., 30, 2226, doi:10.1029/2003GL017969, 2003. 5001

Wunch, D., Toon, G. C., Wennberg, P. O., Wofsy, S. C., Stephens, B. B., Fischer, M. L., Uchino, O., Abshire, J. B., Bernath, P., Biraud, S. C., Blavier, J.-F. L., Boone, C., Bowman, K. P., Browell, E. V., Campos, T., Connor, B. J., Daube, B. C., Deutscher, N. M., Diao, M., Elkins, J. W., Gerbig, C., Gottlieb, E., Griffith, D. W. T., Hurst, D. F., Jiménez, R., Keppel-Aleks, G., Kort, E. A., Macatangay, R., Machida, T., Matsueda, H., Moore, F., Morino, I., Park, S., Robinson, J., Roehl, C. M., Sawa, Y., Sherlock, V., Sweeney, C., Tanaka, T., and Zondlo, M.

AMTD
6, 4999–5031, 2013

A.: Calibration of the Total Carbon Column Observing Network using aircraft profile data, Atmos. Meas. Tech., 3, 1351–1362, doi:10.5194/amt-3-1351-2010, 2010. 5002

Yang, Z., Toon, G. C., Margolis, J. S., and Wennberg, P. O.: Atmospheric CO_2 retrieved from ground-based near IR solar spectra, Geophys. Res. Lett., 29, 1339, doi:10.1029/2001GL014537, 2002. 5001

Yurganov, L. N., Blumenstock, T., Grechko, E. I., Hase, F., Hyer, E. J., Kasischke, E. S., Koike, M., Kondo, Y., Kramer, I., Leung, F.-Y., Mahieu, E., Mellqvist, J., Notholt, J., Novelli, P. C., Rinsland, C. P., Scheel, H. E., Schulz, A., Strandberg, A., Sussmann, R., Tanimoto, H., Velazco, V., Zander, R., and Zhao, Y.: A quantitative assessment of the 1998 carbon monoxide emission anomaly in the Northern Hemisphere based on total column and surface concentration measurements, J. Geophys. Res., 109, D15305, doi:10.1029/2004JD004559, 2004. 5001

Yurganov, L. N., Duchatelet, P., Dzhola, A. V., Edwards, D. P., Hase, F., Kramer, I., Mahieu, E., Mellqvist, J., Notholt, J., Novelli, P. C., Rockmann, A., Scheel, H. E., Schneider, M., Schulz, A., Strandberg, A., Sussmann, R., Tanimoto, H., Velazco, V., Drummond, J. R., and Gille, J. C.: Increased Northern Hemispheric carbon monoxide burden in the troposphere in 2002 and 2003 detected from the ground and from space, Atmos. Chem. Phys., 5, 563–573, doi:10.5194/acp-5-563-2005, 2005. 5001

AMTD
6, 4999–5031, 2013

Table 1. CO null space error for simulated clear-sky measurements using the CO vertical profiles in Fig. 3. For the retrieval, the US standard CO profile is used as reference profile for scaling. The null space error is separated in two contributions, which represents altitude ranges of the averaging kernel with values > 1 (5.7–50 km) and values < 1 (0–5.7 km). All values are given in percent of the true total column.

partial column	high tropos. CO	low tropos. CO
0–5.7 km	+4.13 %	+3.44 %
5.7–50 km	−5.18 %	−6.27 %
0–50 km	−1.05 %	−2.83 %

AMTD
6, 4999–5031, 2013

Table 2. Same as Table 1 but for ozone. Here, the null space error is divided into four contributions (0–9.3 km, 9.3–21.5 km, 21.5–29.5 km, and 29.5–50 km), depending on the values of the column averaging kernel. All values are given in percent of the true total column.

partial column	high O_3	high O_3 + poll.	low. O_3	low O_3 + poll.
0–9.3 km	1.61 %	3.67 %	3.27 %	6.53 %
9.3–21.5 km	−0.63 %	−0.61 %	−0.31 %	−0.29 %
21.5–29.5 km	0.09 %	0.09 %	0.09 %	0.09 %
29.5–50 km	−0.82 %	−0.78 %	−1.02 %	−0.96 %
0–50 km	0.25 %	2.37 %	2.03 %	5.37 %

AMTD
6, 4999–5031, 2013

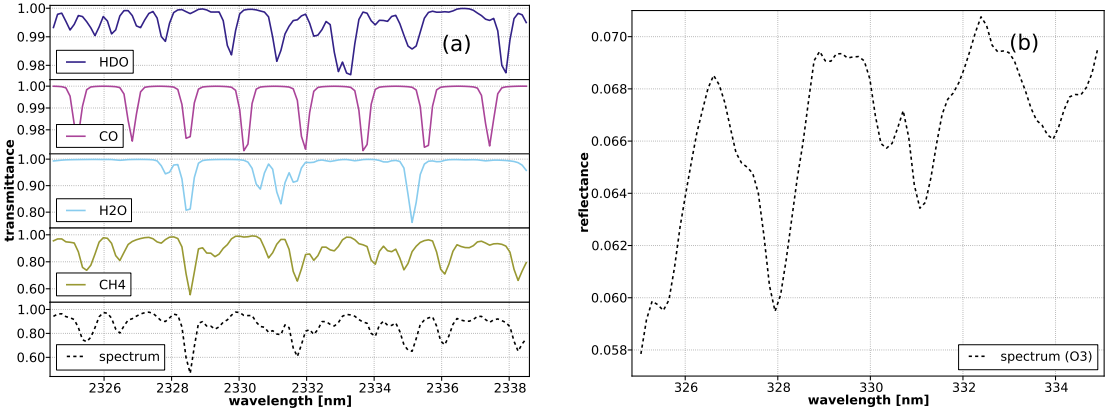

Fig. 1. Simulation of solar absorption spectra. **(a)** CO retrieval window 2324–2339 nm simulated with a spectral resolution of 0.25 nm using HITRAN 2008 spectroscopy (Rothman et al., 2003). The absorptions of the interfering species HDO, H_2O and CH_4 are separated. **(b)** The corresponding O_3 retrieval window 223–336 nm, which employs the Brion et al. (1993) line list database. All simulations are performed for clear-sky condition and a solar zenith angle of 45° and a viewing zenith angle of VZA = 0°.

AMTD
6, 4999–5031, 2013

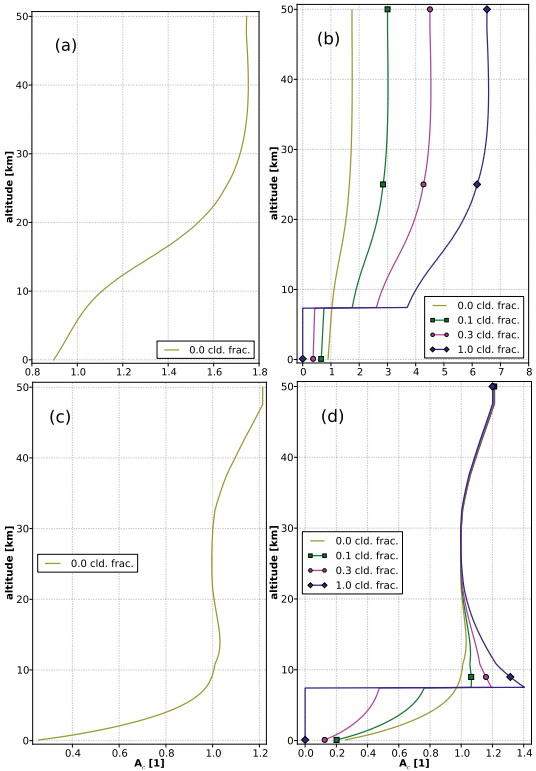

Fig. 2. Total column averaging kernels $\widetilde{A}_C$ of the CO **(a, b)** and O_3 **(c, d)** profile scaling retrieval as function of altitude for different cloud fraction. In the forward calculation a Lambertian surface with albedo 0.5 for SWIR and 0.8 for UV is placed at an altitude of 7.5 km. Measurement geometry and surface albedo are the same as in Fig. 1. The kernels are presented on a vertical grid with 512 equidistant layers.

AMTD
6, 4999–5031, 2013

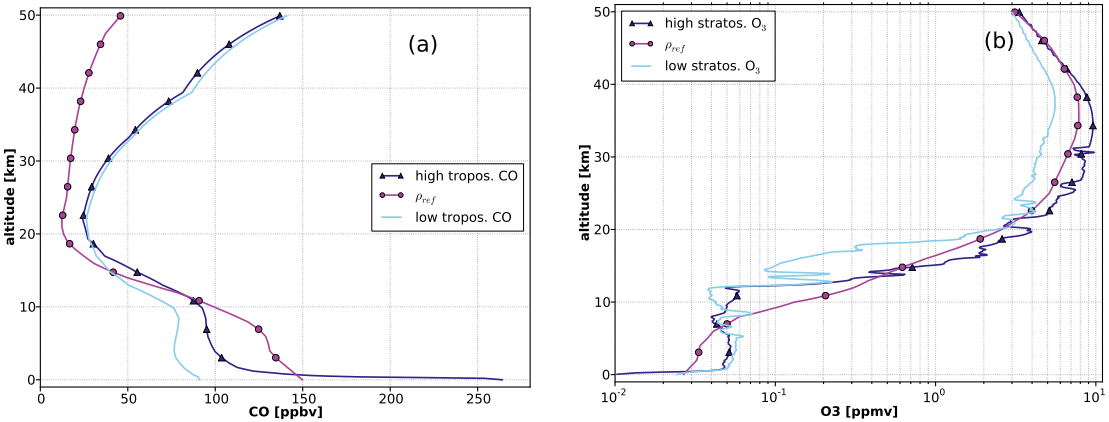

Fig. 3. Ensemble of CO and O_3 volume mixing ratio profiles. **(a)** CO profiles for polluted and unpolluted situations adapted from Levelt et al. (2009) and the CO profile taken from the US standard atmosphere (NOAA, 1976). **(b)** Two O_3 radiosonde measurements at de Bilt, the Netherlands, with high (16 February 2007) and low stratospheric O_3 (19 February 2008). Additionally, the US standard atmosphere ozone profile is depicted.

AMTD
6, 4999–5031, 2013

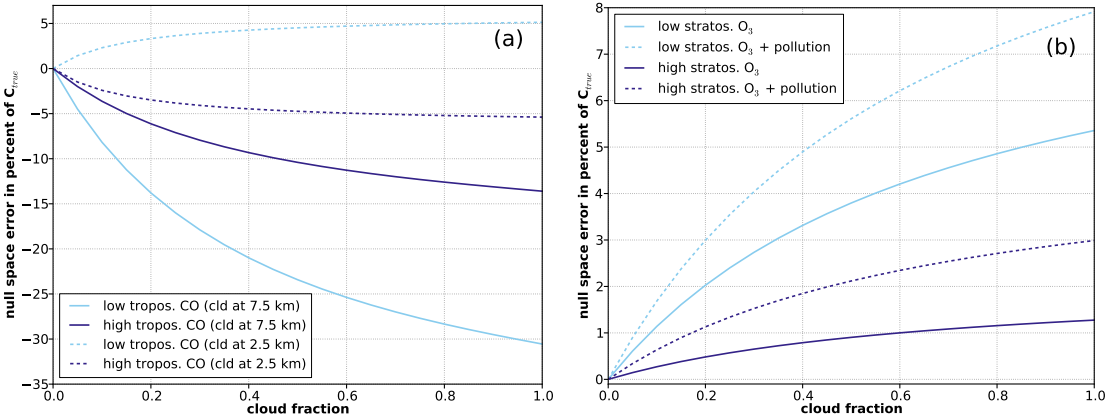

Fig. 4. Null space error for cloudy scenes as a function of cloud fraction: **(a)** CO null space error for the background and polluted CO profile shown in Fig. 3 for a cloud at 7.5 and 2.5 km, **(b)** O_3 null space error for high and low stratopsheric ozone profiles shown in Fig. 3 respectively with and without a pollution of 120 ppb in the boundary layer. Values are given in percentage of the known true total column. The difference to the clear-sky case is shown.

AMTD
6, 4999–5031, 2013

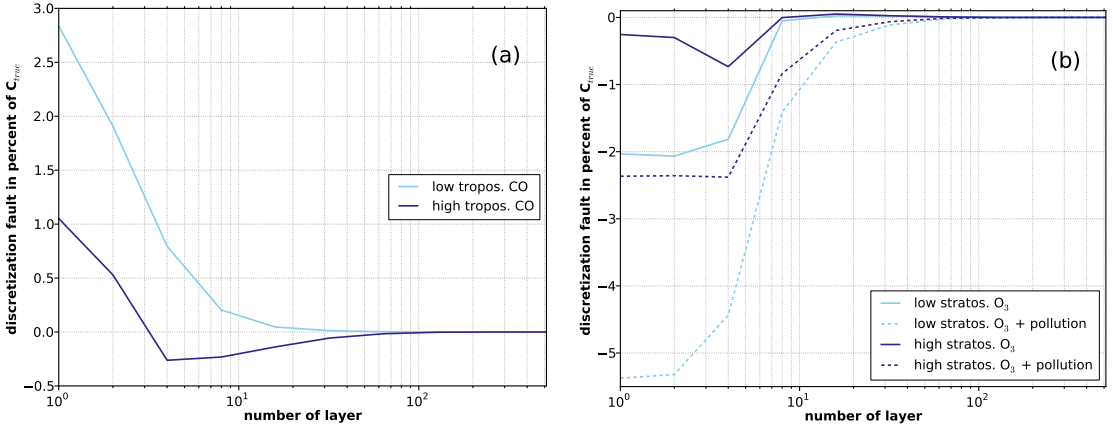

Fig. 5. Discretization error of the null space error for **(a)** CO and **(b)** O_3 caused by representing the total column averaging kernel on an equidistant vertical grid with N layer. It is shown how the retrieved column calculated on N layers deviates from the one calculated on 512 layers. Values are given in percentage of the known true total column.

AMTD
6, 4999–5031, 2013